

Surface Effects in Ferroelectrics: Periodic Slab Computations for **BaTiO₃**

R. E. Cohen

Carnegie Institution of Washington, 5251 Broad Branch RD., N.W., Wahsington

D.C. 20015

(December 2, 2024)

Abstract

Total energies, electronic structure, surface energies, polarization, potentials and charge densities were studied for slabs of BaTiO₃ using the Linearized Augmented Plane Wave (LAPW) method. The depolarization field inhibits ferroelectricity in the slabs, and the macroscopic field set up across a ferroelectric slab is sufficient to cause electronic states to span the gap and give a metallic band structure, but the band shifts are not rigid and O *p* states tend to pile up at the Fermi level. There are electronic surface states, especially evident on TiO₂ surfaces. The dangling bonds bond back to the surface Ti's and make the surface stable and reactive. The BaO surfaces are more ionic than the bulk.

I. INTRODUCTION

Surfaces of ferroelectrics can strongly effect their properties. In general this is a much stronger effect than in paraelectric materials, because the termination of a ferroelectric gives rise to a depolarization field, which is huge in an ideal, ionic ferroelectric. The depolarization field, E_d , is opposite in sign to the bulk polarization, and gives a contribution to the energy of $-E_d \cdot P$ large enough to completely destabilize the bulk ferroelectric state^{1,2}. The ferroelectric

distortion in thin films varies with thickness so that the structures become cubic at thin edges³. Huge particle size effects are observed^{4,5}, orders of magnitude greater than observed for non-ferroelectrics. Surfaces are important also during crystal growth, and their properties are key to catalysis and use as an epitaxial substrate. Here we study thin slabs of BaTiO₃ to better understand the electronic structure of the surface, surface energetics and relaxation, and intrinsic screening of the depolarization field.

Experimental studies of BaTiO₃ surfaces are few and many more studies have focused on SrTiO₃ which lacks the complications of ferroelectricity. Photoemission studies of sputtered and annealed BaTiO₃ show evidence of significant surface defects⁶, and a number of papers have addressed the defect properties of the surface^{7–9}. Studies of SrTiO₃ surfaces show evidence for minor relaxations by motions of atoms perpendicular to the surfaces^{10,11} and show no evidence for states in the gap.¹² Some recent studies of BaTiO₃ show evidence for gap states⁸, and others do not¹³, probably indicating sensitivity to the surface defect state. Photoemission spectroscopy on BaTiO₃ shows excellent agreement with bulk LAPW computations of the LDA band structure¹³.

First-principles electronic structure approaches have been very successful for bulk ferroelectrics^{14–21} but the application of first-principles band structure methods to surface properties is daunting due to the giant computational burden. Here the first set of accurate electronic structure calculations for periodic BaTiO₃ slabs are presented. These results can be considered benchmark results for faster, more approximate methods, and also give some insights into the electronic structure of ferroelectric BaTiO₃ surfaces.

II. METHOD

We studied six to seven atomic layer (001) and (111) periodic slabs of BaTiO₃ containing 15–18 atoms in the periodic unit, with seven to six layers of vacuum, using the Linearized Augmented Plane Wave method with extra local orbitals (LAPW+LO) method.²² Both slabs were studied in the ideal configuration, and the more stable (001) slab was studied

extensively with tetragonal ferroelectric distortions and with surface relaxations. In each case the in-plane lattice constant was 7.57 bohr ($=4.006 \text{ \AA}$). An ABO_3 perovskite slab can have two types of terminations, AO (Type I) and BO_2 (Type II). Three configurations for the (001) slab were studied, asymmetrically terminated (BaO and TiO_2 surfaces), and symmetrically terminated with BaO and TiO_2 surfaces, respectively. The slabs in each case were repeated with periodic boundary conditions. The (001) slab had a repeat length of six times the cubic lattice constant, or 45.42 bohr ($=24.035 \text{ \AA}$); whereas for the (111) slab $a=10.70$ bohr $c=26.2$ bohr. The ideal slabs are illustrated in figure 1. The (001) slab has P4mm tetragonal symmetry with eight-space group operations, and the (111) slab is rhombohedral with R3m symmetry. In order to obtain accurate energy differences and surface energies, bulk calculations were also performed in the same symmetry with a tripled supercell with the same k-points and convergence parameters.

The ferroelectric distortion in the (001) slab used the experimental tetragonal average displacements. The Ba's were displaced by 0.06 \AA , the Ti's by -0.1122 \AA along c relative to the O(II)'s, and the O(I)'s by 0.0288 \AA . For the asymmetrically terminated slab, displacements were performed in both directions, with Ti displaced towards the Ba-O surface (+) and towards the Ti-O surface (-). The tetragonal phase in bulk BaTiO_3 does not consist primarily of displacements towards the perovskite cube faces, as we are studying here, but rather displacements towards the cube diagonals, and the tetragonal structure is a dynamical average with hopping among four (111) directions. Such disordered configurations are well beyond the possibilities of present computations for slabs, and must await future faster and probably more approximate methods. Nevertheless, the general effects of a surface on ferroelectric properties can be illuminated by the present study.

The surface layers were relaxed using the LAPW forces²³ and a quasi-Newton method for the ideal (001) Ba-Ti terminated slab, the ferroelectric (+) Ba-Ti terminated slab, and the ferroelectric Ba-Ba terminated slab.

The convergence parameter RK_{max} was set to 7.0; Table I shows the muffin tin radii. A $4\times4\times2$ special k-point mesh was used which gives 3 k-points for the (001) slab and

10 k-points for the (111) slab. The ferroelectric Ba-Ti slab was also converged with a $6 \times 6 \times 2$ mesh (6 k-points) and the total energy for the 15 atom unit cell only differed by 0.2 mRyd. The matrix order (number of basis functions) for the slabs was about 2900 for the first k-point set (see Table I) and 3800 for the second k-point set. These calculations are extremely computationally intensive. Not only was each iteration in the self-consistent cycle time consuming but an unusually large number of iterations were required to reach self-consistency due to charge fluctuations across the slab set up by the electric fields generated across the slab.

III. RESULTS AND DISCUSSION

Table I shows the unrelaxed and relaxed (001) slab structures, and total energies for all studied slabs are shown in Table II. Since the (111) slab is found to be much more unstable than the (001) slab, most of the computations and the discussion below concentrate on the (001) slab. Whereas there is a ferroelectric instability, or double well, found for bulk BaTiO_3 , there is no ferroelectric instability for the slab. Rather the energy increases with ferroelectric distortion due to the depolarization field that forms at the surface. This is the same result that was obtained using an ionic model for finite clusters.² Furthermore, for the asymmetrically terminated Ba-Ti slab, the energy is not symmetric with respect to “+” and “-” ferroelectric distortions, with a much lower energy being obtained when the Ti atoms are moved so that the partially coordinated surface Ti atoms move in towards the slab (“+” distortion in Table II).

A. Relaxation

The surface relaxations can be described as a combination of relaxation of the surface layer in towards the slab, and a dimpling of the layers. Here we define the former by the motion of the midpoint between the z coordinate for the surface cation and anion relative to that of the ideal interlayer spacing, and the latter by half of the difference in z-coordinate of

the surface ions. In agreement with work on other oxides, the sign of the rumpling is such that the surface cations move in towards the slab and the anions move out (Table III). The sign of the effect is independent of the slab termination or whether the slab is ferroelectric or ideal. The magnitude of the rumpling is quite similar to that obtained experimentally for SrTiO_3 .¹⁰ However, the experiment did not resolve net relaxation of the layer spacing, whereas we find that the surface layer spacing is contracted relative to that of the bulk spacing. This may be partly due to the fact that we did not relax all of the atomic positions in the bulk of the slab, but rather fixed the interlayer spacing at the experimentally observed zero pressure value, and LDA gives a smaller lattice constant than experiment for the bulk. The relaxations are energetically significant as is shown in Table II: 0.032 Ryd for the ideal (001) Ba-Ti terminated slab, 0.016 Ryd for the ferroelectric Ba-Ti terminated slab, and 0.026 Ryd for the ferroelectric Ba-Ba terminated slab. For the Ba-Ti slab the relaxation energy per surface is about 16% of the cleavage energy.

B. Surface energies

Only the symmetrically terminated ideal slabs are expected to give accurate estimates of the surface energy, because the asymmetrically terminated and ferroelectric slabs have potential gradients (net polarization or macroscopic electric field E_{mac}) which adds a term to the energy proportional to E_{mac}^2 . It is necessary to consider both the BaO and TiO_2 terminated slabs together, since neither alone has bulk stoichiometry, and thus its energy cannot be compared with bulk. Thus if we add the energies of the BaO terminated slab and the TiO_2 terminated slab, we get -128935.8994 Ryd for 7 BaTiO_3 units and 4 surfaces (2 BaO and 2 TiO_2). We subtract 7 times the bulk BaTiO_3 energy per cell (-128936.1703 Ryd) and get 0.2709 Ryd for 4 surfaces, or an average of 0.0677 Ryd/surface, which gives 0.0574 eV/ \AA^2 ($=2712 \text{ erg/cm}^2 = 0.92 \text{ J/m}^2$). For comparison, the unrelaxed surface energy for Cr_2O_3 is estimated to be 2000 erg/cm² for the relaxed surface²⁴. The surface energy of SiO_2 glass is much lower, about 300 erg/cm². We have not relaxed the symmetric TiO_2

terminated slab, but if its relaxation energy is similar to that of the three slabs we did relax, relaxation would lower the surface energy by about 12%. The very high surface energy for BaTiO₃ explains why it does not cleave easily, but rather fractures. Real BaTiO₃ surfaces are probably highly defective and measured surface energies may be therefore lower.

C. Electronic structure

Fig. 2 shows the calculated band structures the band structure of the unrelaxed asymmetrically terminated Ba-Ti slab, the slab with surface layers relaxed, and for bulk BaTiO₃ folded into the tripled Brillouin zone of the slab. The relaxation makes small changes in the band structure, but they are difficult to see on the scale shown. The top valence band and bottom conduction band of the slab are interface states. The nature of these states is clearer from Fig. 3 where the band structures for the unrelaxed symmetrically terminated BaO and TiO₂ slabs are shown. The occupied interface state is due to the TiO₂ surfaces, and the interface state for the conduction band is primarily due to the BaO surface.

The density of states was computed using the tetrahedron method with Fourier interpolation²⁵ from a k-point mesh of $8 \times 8 \times 2$ to a $16 \times 16 \times 4$ mesh in the full Brillouin zone. Fig. 4 shows the density of states for the ferroelectric BaO symmetrically terminated slab. There are Ba p -O p hybrid occupied surface states, and an unoccupied O p band also comes down about 0.5 eV lower than the bulk band. The Ba p states look quite different on the surface than in the bulk, and in fact appear to be significantly less hybridized than the bulk Ba, indicated than Ba is even more of a perfect 2+ ion on the surface than in the bulk. The main valence band states on the surface O are significantly less bound than the bulk O, with more weight at the top of the valence band. Fig. 5 shows that the occupied surface states on TiO₂ surfaces have primarily O p character, with some hybridization, interestingly, with the neighboring Ba in the next layer. Fig. 6 shows the density of states for the unrelaxed and relaxed ferroelectric BaO symmetrically terminated slab. The ferroelectric displacement sets up a potential gradient across the slab (a net macroscopic field) that

shifts the bands as a function of position in the slab. In fact, the experimental ferroelectric displacement generates a potential gradient large enough to make the slab metallic even for the thin slabs studied here. The Ti d-states at the bottom of the slab become partially occupied and the O p and Ba p states become partially empty at the other end of the slab. Most interestingly, the bands do not move rigidly. It appears that the O 2p states really do not want to be partially occupied, and these states “pile up” against the Fermi level. The fact that this is energetically preferred rather than allowing the oxygen to become partially charged and highly nonspherical indicates how strongly the O atoms are stabilized in the closed shell configuration, even on the surface of a slab. What is so surprising about this is that O^{2-} is not even stable in the free state; it is only stabilized due to the Madelung (electrostatic) field from the rest of the crystal. This is not an theoretical artifact; free O^{2-} is unstable and decays to $O^- + e^-$. It appears that this stabilization is strong enough even on the BaO perovskite surface. The charge transfer across the slab screens partially screens the field, so that the gap is just closed, as is discussed further below.

In band theory as applied here, there is a constant Fermi level and states are occupied up to it. In an ideal insulating slab or crystal in a field, however, the situation would be different and the Fermi level would vary with macroscopic position and charge would not flow since states would not communicate over macroscopic distances except by tunneling which is very slow. This is similar to a hydrogen atom in an electric field; the ground state for an infinitesimal field is for the electron to be stripped off, but this does not happen even over long times due to a long lifetime for the metastable state. In a real slab or crystal, however, there are extrinsic or thermally induced defects so the conductivity is finite. Charge flow thus would occur and the results would be similar to what we obtain here in the static limit.

D. Analysis of potential and charge densities

Figure 7a shows the charge density of the asymmetrically terminated ideal slab with overlapping spherical ions subtracted. On the TiO_2 surface the O p charge density, instead

of dangling, bonds back to the surface Ti's. In other words, the surface charge density is self-healing. The bonds between the O and Ti are clearly evident. Most interesting is the collapse of the surface Ti bond. Instead of dangling the charge moves back onto the Ti and the Ti-O surface bonds. This self-healing leaves the surface highly reactive but stable (i.e. it doesn't reconstruct), and is probably responsible for the utility of BaTiO₃ as a substrate for epitaxial growth and for surface catalysis. The Ba-O surface shows much less difference from spherical ions, and is found to be highly ionic. These results suggest that the Ti-O surface of BaTiO₃ is highly reactive due to the possibility of covalent bonding on the surface, whereas any reactivity Ba-O surface is due entirely to ionic bonding. The non-bonding O p surface state may also enhance surface reactivity.

Figure 7b shows the difference between the LAPW (001) slab density and the self-consistent LAPW charge density for bulk periodic BaTiO₃. Large changes are seen on the surface Ti, and smaller changes on the surface Ba and O. Most interestingly, the differences the interior Ti and O, which are only one unit cell away from the surface, are almost identical to bulk Ti and O. This shows that electronic perturbations due the surface are screened very rapidly in the interior of a crystal. The screening is accomplished primarily due to polarization and charge redistributions around the surface Ti, and to a lesser extent, O ions.

In order to understand the polarization and depolarization fields of the slab, we now examine the total potentials averaged in the x-y plane as a function of z-coordinate in the slabs. Figure 8 shows the potential for the symmetric BaO terminated ideal and ferroelectric slabs. There is no net field in the vacuum region in the ideal case, and the field is a constant 0.015 Ryd/bohr in the vacuum in the ferroelectric case. The results for the asymmetrically terminated slabs are much more complicated, since a field is present in the vacuum even in the ideal case (Fig. 9). The existence of the field in this case can be thought of as due to different work functions for the BaO and TiO₂ surfaces, but in any case it indicates that the slab has a net dipole moment in spite of the fact that if one considers the nominal charges (2+, 4+ and 2- for Ba, Ti and O respectively), the TiO₂ and BaO planes would be charge

balanced and the ideal slab would have no net polarization. One possible explanation of the result is that a surface charge develops due to the surface states. This possibility was tested by comparing the charge densities of the asymmetrically terminated slab with the symmetrically terminated BaO and TiO₂ slabs, but no evidence for a surface charge could be found. The implication is that even in the bulk the BaO and TiO₂ planes do not carry the same charge.

The above analysis allows the field to be easily extracted from the vacuum region, but does not easily allow extraction of the macroscopic field in the slab since the potential is dominated by local contributions from the atoms. We can extract macroscopic field effects in the slabs by examining deep core states. In figure 10 the O 1s core levels are shown as a function of position in the symmetrically terminated BaO slab. As expected there is no net field in the ideal slab, but there is a nearly constant macroscopic field as determined from the O 1s levels in the ferroelectric slab. The picture in the asymmetrically terminated slab is again complicated (Fig. 11). The net field as seen in the center of the asymmetrically terminated ideal slab is very small, in spite of the large field in the vacuum. The field for the ferroelectric relative to the ideal asymmetric slab is nearly constant, and is about 0.01 Ryd/bohr.

We can understand better the observed macroscopic fields by considering the ideal case of a periodic slab of thickness L_1 separated by vacuum regions of thickness L_2 with constant fields E_1 and E_2 in the two regions. The electric displacements are given by $D_1 = E_1 + 4\pi P_1$ in the slab and $D_2 = E_2$ in the vacuum, where P_1 is the total polarization in the slab, including the spontaneous polarization P_s and the induced polarization $P_i = (\varepsilon_1 - 1)E_1/4\pi$. Now $D_1 = D_2$ and $E_1L_1 + E_2L_2 = 0$ since the potential must be continuous. For the BaO terminated slab we get $E_1 = 0.005$ H/bohr and $E_2 = -0.0073$ H/bohr which gives $L_1/L_2 = 1.45$, which compares well with the simple consideration of 7 slab layers and 5 vacuum layers, or $L_1/L_2 = 1.4$, indicating that our method of estimating E_1 and E_2 from the vacuum potential and the O 1s core levels is consistent. Using the experimental dielectric constant $\varepsilon = 5.24$ we get $P_s = 15 \mu\text{C}/\text{cm}^2$, which is significantly lower than the experimental

value of $26 \mu\text{C}/\text{cm}^2$. The screening caused by the metallic band structure is most likely the major cause of this difference. This has important implications, and shows that with finite conductivity, a ferroelectric will self-screen the depolarization field, because of the effective closing of the gap from one part of a ferroelectric domain to the other. Many of the implications remain to be worked out.

Finally, we consider the magnitude of the depolarization energy, $W_D = \frac{1}{2} \int D \cdot E \, dV$. For the ferroelectric symmetrically terminated BaO slab we find $W_D = 0.055 \text{ Ryd} (= 0.75 \text{ eV})$, a large energy which easily overcomes the energy lowering for the ferroelectric distortion in bulk BaTiO₃ of 0.015 eV per unit cell, or 0.053 eV for the equivalent number of atoms as the slab contains in a periodic unit by a factor of about 14. Note that both numbers scale up with size, so even macroscopic crystals must break up into domains, or the depolarization field must be pacified by formation of a surface space charge.

IV. CONCLUSIONS

We have studied ferroelectric and ideal slabs of BaTiO₃ using the full-potential all-electron LAPW method. Surface relaxations are significant, and similar to what is observed for SrTiO₃. There are significant surface states, especially on the TiO₂ surfaces. The dominant surface state has O p character, and seems to be related to the collapse of the dangling bonds back onto the surface Ti ions. The charge density in the center of the slab is very close to the charge density in bulk BaTiO₃. We find the asymmetrically terminated slabs have significant potential gradients (electric fields) in the vacuum due to the different net charges on BaO and TiO₂ planes. Most interestingly, we find that the ferroelectric slabs are metallic due to potential shifts that are greater than the band gap. The bands, however, do not shift in a rigid way; rather the O 2p states pile up at the Fermi level showing that the O atoms prefer to remain closed-shelled, even on the surface. The metallic nature of the ferroelectric slabs screens the macroscopic polarization, so we find a polarization smaller than the experimental bulk value. The depolarization field is large and inhibits ferroelectricity.

In order to recover a ferroelectric state, this field must be screened or the crystal must break up into domains.

ACKNOWLEDGMENTS

Thanks to V. Heine, I. Mazin, R. Resta, and D. Vanderbilt for helpful discussions and suggestions on how to interpret the slab results. D. Vanderbilt suggested the study of symmetrically terminated slabs which was very useful. This research is supported by the Office of Naval Research. Computations were performed on the Cray J90 at the Geophysical Laboratory..

TABLES

TABLE I. Structures of (001) BaTiO₃ slabs (z coordinates shown only, in lattice coordinates, $c=24.035$ Å). Only relaxed coordinates are shown for partially relaxed structures.

atom	x,y	termination	ideal	relaxed	ferro -	ferro +	relaxed	ideal	ferro	relaxed	ideal
		Ba-Ti	Ba-Ti	Ba-Ti	Ba-Ti	Ba-Ti	Ba-Ba	Ba-Ba	Ba-Ba	Ti-Ti	
Ba	0,0		0	0.00715	0.0025	-0.0025	0.00596	0	-0.0025	0.00762	0
Ba	0,0			0.16667		0.16917	0.16417		0.16667	0.16417	0.16667
Ba	0,0			0.33333		0.33583	0.33083		0.33333	0.33083	0.33333
Ba	0,0							0.5	0.50128	0.49110	
Ti	0.5,0.5										-0.08333
Ti	0.5,0.5		0.08333		0.088	0.07867		0.08333	0.07867		0.08333
Ti	0.5,0.5		0.25		0.25467	0.24533		0.25	0.24533		0.25
Ti	0.5,0.5		0.41667	0.40868	0.42133	0.412	0.40910	0.41667	0.412		0.41667
O	0,0						0	0.00128			-0.08333
O	0.5,0.5		0	0.00544	-0.00128	0.00128	0.00241	0.08333	0.08333	0.00276	0
O	0,0		0.08333		0.08333	0.08333		0.16667	0.16795		0.08333
O	0.5,0.5		0.16667		0.1653	0.16795		0.25	0.25		0.16667
O	0,0		0.25		0.25	0.25		0.33333	0.33462		0.25
O	0.5,0.5		0.33333		0.332	0.33462		0.41667	0.41667		0.33333
O	0,0		0.41667	0.41219	0.41667	0.41667	0.41312	0.5	0.50128	0.49199	0.41667

TABLE II. Summary of total energies for BaTiO_3 slabs and bulk.

	Termination	E Ryd/cell
symmetric bulk (3 (001) layers) ^a		−55258.3586
symmetric bulk (2 (111) layers) ^a		−55258.3578
ideal (001) slab ^a	Ba-Ti	−55258.1189
ideal (111) slab ^a	Ba-Ti	−55257.4260
ferroelectric slab (−) ^a	Ba-Ti	−55258.0482
ferroelectric slab (+) ^a	Ba-Ti	−55258.1119
symmetric bulk (3 (001) layers) ^b		−55258.4348
ideal (001) slab ^b	Ba-Ti	−55258.2119
(001) slab relaxed ^b	Ba-Ti	−55258.2434
ferroelectric slab (+) ^b	Ba-Ti	−55258.2063
ferroelectric slab (+) relaxed ^b	Ba-Ti	−55258.2222
ideal (001) slab ^b	Ba-Ba	−71674.0910
ferroelectric (001) slab ^b	Ba-Ba	−71674.0495
ferroelectric (001) slab relaxed ^b	Ba-Ba	−71674.0758
ideal (001) slab ^b	Ti-Ti	−57261.8084

^aMuffin tin radii: Ba=2.3 bohr, Ti=1.75 bohr, O=1.75

^bMuffin tin radii: Ba=2.3 bohr, Ti=1.59938 bohr, O=1.59938

TABLE III. Summary of relaxations of surface layers in Å.

	Ba-Ti ideal	Ba-Ti ferro +	Ba-Ba ferro	SrTiO ₃ ^b
relaxation of Ba-O layer	0.15	0.12	0.14	-0.08
change in dimpling of Ba-O layer	0.02	0.088 ^a	0.10 ^a	0.08
relaxation of Ti-O layer	0.15	0.078	0.23	-0.05
change in dimpling of Ti-O layer	0.08	0.0078	0.011	0.05

^aSign of dimpling changes relative to ferroelectric distortion.

^bRef.¹⁰

FIGURES

FIG. 1. Structures of slabs studied. (a) (111) slab (b) (001) slab. Blue is oxygen, green is Ba, and red is Ti. Ti-O bonds are shown in black.

FIG. 2. Band structures for (a) undistorted bulk BaTiO_3 folded into the Brillouin zone for the three layer slab, and (b) for the assymetrically terminated slab with BaO and TiO_2 surfaces. The bands for the unrelaxed ideal slab are shown as solid lines, and for the slab with relaxed surfaces are dashed.

FIG. 3. Band structures for symmetric (a) BaO and (b) TiO_2 terminated ideal slabs. The highest valence band in (b) is a surface state with O 2p character, and the lowest conduction band in (a) is also a surface state with primarily O 2p character.

FIG. 4. Partial density of states for the symmetric ideal BaO terminated slab. Note the different scales for Ba p and Ti d. The Fermi level is shown as the vertical dashed line. The amount of Ti hybridization with O 2p is about constant through the slab, but the Ba p hybridization is lower on the surface than in the bulk. The O 2p bands are correspondingly wider in the bulk than on the surface. The surface is more ionic than the bulk.

FIG. 5. Partial density of states for the symmetric ideal TiO_2 terminated slab. There is a significant surface state with O 2p character as was shown in fig. 3. The surface seems slightly more ionic than the interior of the slab, and the Ti d states are slightly less bound.

FIG. 6. Partial density of states for the ferroelectric symmetrically BaO terminated slab. The Ti displacements were towards the bottom of the slab (corresponding to the bottom panels). The solid line is for the ideal ferroelectric slab with the experimental tetragonal displacement pattern, and the dashed line is for the slab with relaxed surface atoms. The slab is metallic, with conduction bands crossing the Fermi level at the bottom of the slab and O 2p states and Ba p states crossing the Fermi level at the top of the slab. Note that the bands are displaced due to the ramp potential across the slab, but the band shifts are not rigid. Rather the O 2p density piles up at the Fermi level at the top of the slab, indicating that the O ion want to remain a closed shell. Only a small amount of charge transfer occurs in order to screen the macroscopic field to the point that the gap is just closed.

FIG. 7. Charge density for BaTiO₃ slab. (a) Deformation charge density for BaTiO₃. The image shows the difference in charge density between the self-consistent LAPW charge density and overlapping PIB ions. Green represents no change in density (i.e. identical to the ionic crystal). Partially charged ions, Ba^{1.63+}, Ti^{3.26+}, O^{1.63-} were used to generate the ionic charge density. Note the “healing” of the surface Ti dangling bond. It collapses back onto the Ti. (b) Difference in charge density between the ideal slab and bulk BaTiO₃. Even though the slab is only three layers thick, the central layer has almost an identical charge density to bulk BaTiO₃, although there are still some small differences on the Ba.

FIG. 8. Total potential averaged in the x-y plane as a function of z for the symmetric ideal and ferroelectric BaO terminated slabs. The average field is zero in the vacuum between slabs in the ideal case, and is 0.39 eV/Å in the ferroelectric case. The experimental tetragonal displacement pattern is used.

FIG. 9. Electric field shown only in the vacuum region for the asymmetrically terminated slabs.

FIG. 10. Core levels for symmetric BaO terminated slabs. (a) O 1s core energies as a function of layer (z coordinate) in slabs for ideal and ferroelectric slab. (b) Macroscopic electric field derived from changes in core levels.

FIG. 11. Core levels for asymmetrically terminated slabs. (a) O 1s core energies as a function of layer (z coordinate) in slabs for ideal and ferroelectric slabs, relaxed and unrelaxed. (b) Macroscopic electric field derived from changes in core levels.

REFERENCES

¹ M.E. Lines and A.M. Glass, *Principles and Applications of Ferroelectrics and Related Materials*, (Clarendon Press, Oxford, 1977).

² Z. Gong and R.E. Cohen, *Ferroelectrics*, **136**, 113 (1992).

³ F. Tsai and J.M. Cowley, *Appl. Phys. Lett.* **65**, 1906 (1994).

⁴ J.C. Niepce, in *Surfaces and Interfaces of Ceramic Materials*, edited by L.-C. Du-four.(Kluwer, 1989), 521-533,

⁵ K. Uchino, E. Sadanaga, K. Oonishi, and H. Yamamura, *Ceramic Transactions*, **8**, 107 (1990).

⁶ B. Cord and R. Courths, *Surface Science*, **152/153**, 1141 (1985).

⁷ H. Bando, T. Shimitzu, Y. Aiura, Y. Haruyama, K. Oka, and Y. Nishihara, *J. Vac. Sci. Technol.* **14**, 1060 (1996).

⁸ S.M. Mukhopadhyay and T.C.S. Chen, *J. Mat. Res.* **10**, 1502 (1995).

⁹ T. Shimizu, H. Bando, Y. Aiura, Y. Haruyama, K. Oka, and Y. Nishihara, *Jpn. J. Appl. Phys. Lett.* **34**, L1305 (1995).

¹⁰ T. Hikita, T. Hanada, and M. Kudo, *Surface Science*, **287/288**, 377 (1993).

¹¹ J.P. LaFemina, *Critical Reviews in Surface Chemistry*, **3**, 297 (1994).

¹² R.A. Powell and W.E. Spicer, *Phys. Rev. B*, **13**, 2601 (1976).

¹³ S.W. Robey, *Ferroelectrics*, **in press**, (1996).

¹⁴ R.E. Cohen, *Ferroelectrics*, **150**, 1 (1993).

¹⁵ R.E. Cohen, *Nature*, **358**, 136 (1992).

¹⁶ R.E. Cohen and H. Krakauer, *Ferroelectrics*, **136**, 65 (1992).

¹⁷ W. Zhong and D. Vanderbilt, Phys. Rev. Lett. **74**, 2587 (1995).

¹⁸ W. Zhong, D. Vanderbilt, and K.M. Rabe, Phys. Rev. Lett. **73**, 1861 (1994).

¹⁹ W. Zhong, R.D. Kingsmith, and D. Vanderbilt, Phys. Rev. Lett. **72**, 3618 (1994).

²⁰ R. Yu and H. Krakauer, Phys. Rev. Lett. **74**, 4067 (1995).

²¹ D. Singh, Ferroelectrics, **164**, 143 (1995).

²² D.J. Singh, *Planewaves, Pseudopotentials, and the LAPW Method*, (Kluwer Academic Publishers, Boston, 1994).

²³ R. Yu, D. Singh, and H. Krakauer, Phys. Rev. B, **43**, 6411 (1991).

²⁴ P.J. Lawrence and S.C. Parker, in *Computer Modelling of Fluids Polymers and Solids*, , edited by C.R.A. Catlow, S.C. Parker, and M.P. Allen.(Kluwer Academic Publishers, Boston, 1990), 219-248,

²⁵ W.E. Pickett, H. Krakauer, and M.P. Allen, Phys. Rev. B, **38**, 2721 (1988).

This figure "Fig1.gif" is available in "gif" format from:

<http://arxiv.org/ps/mtrl-th/9609002v1>

Fig. 2 Cohen

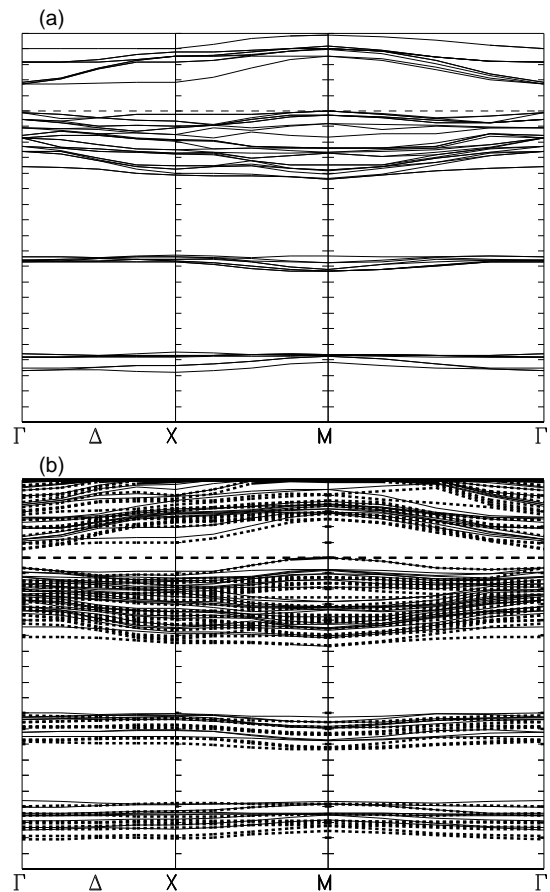


Fig. 3 Cohen

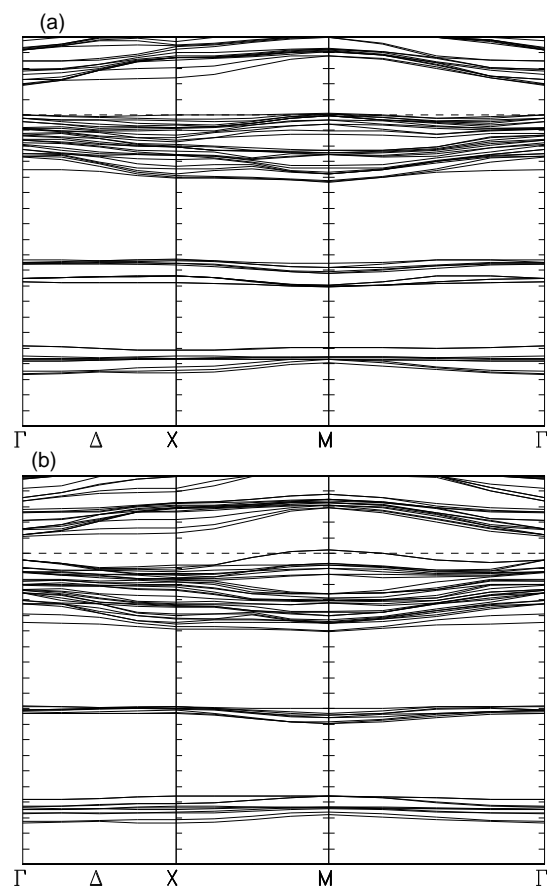


Fig. 4 Cohen

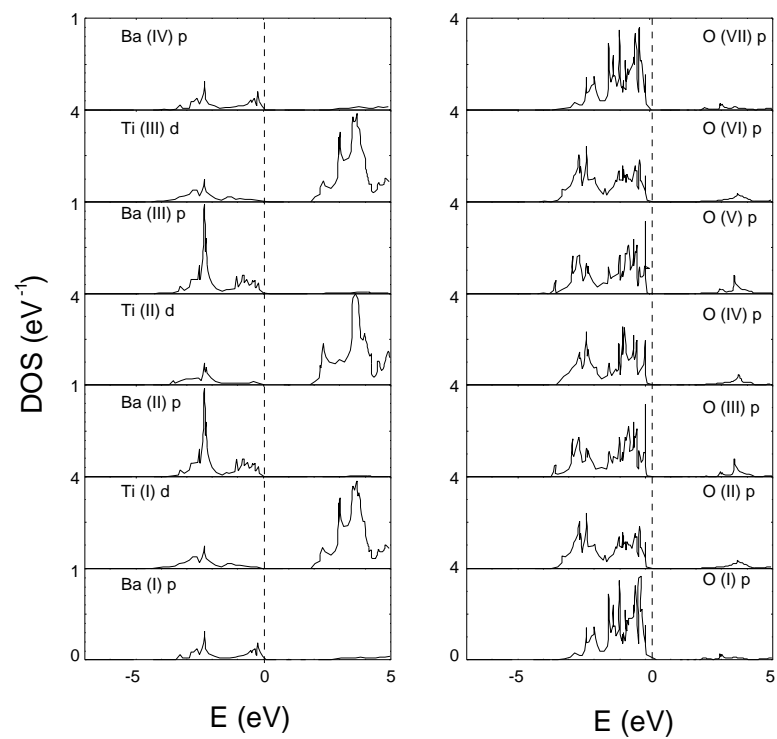


Fig. 5 Cohen

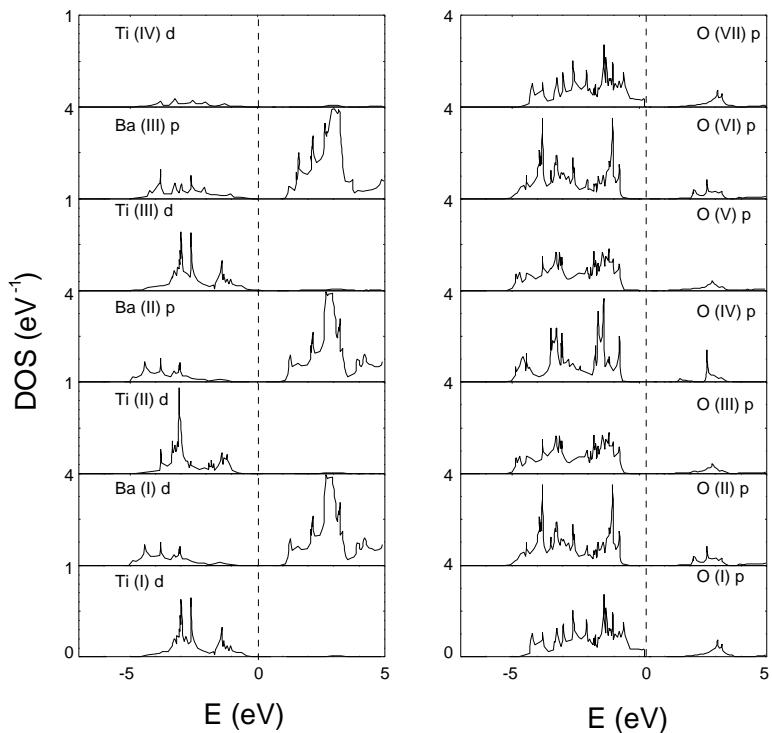
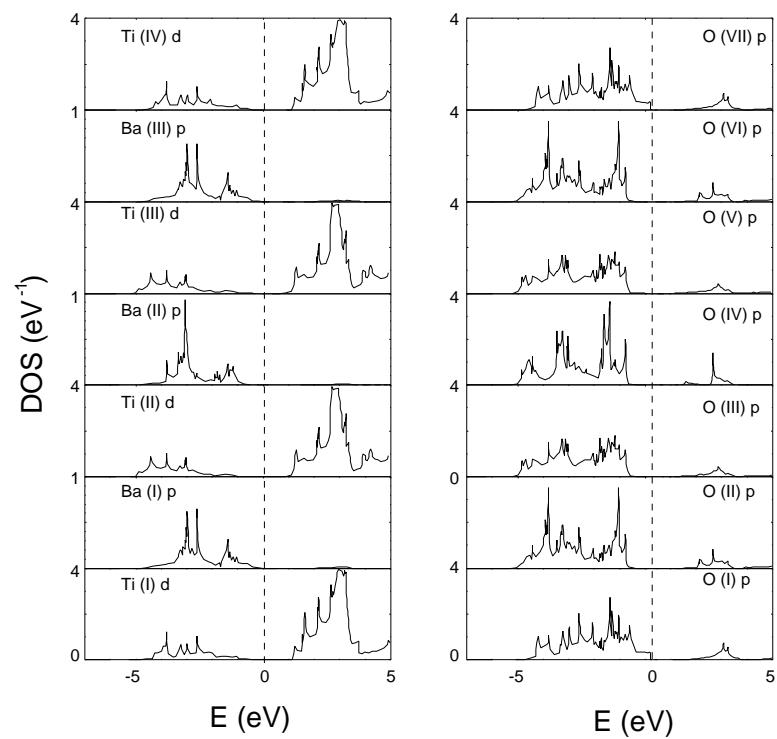


Fig. 6 Cohen



This figure "Fig7.gif" is available in "gif" format from:

<http://arxiv.org/ps/mtrl-th/9609002v1>

Fig. 8 Cohen

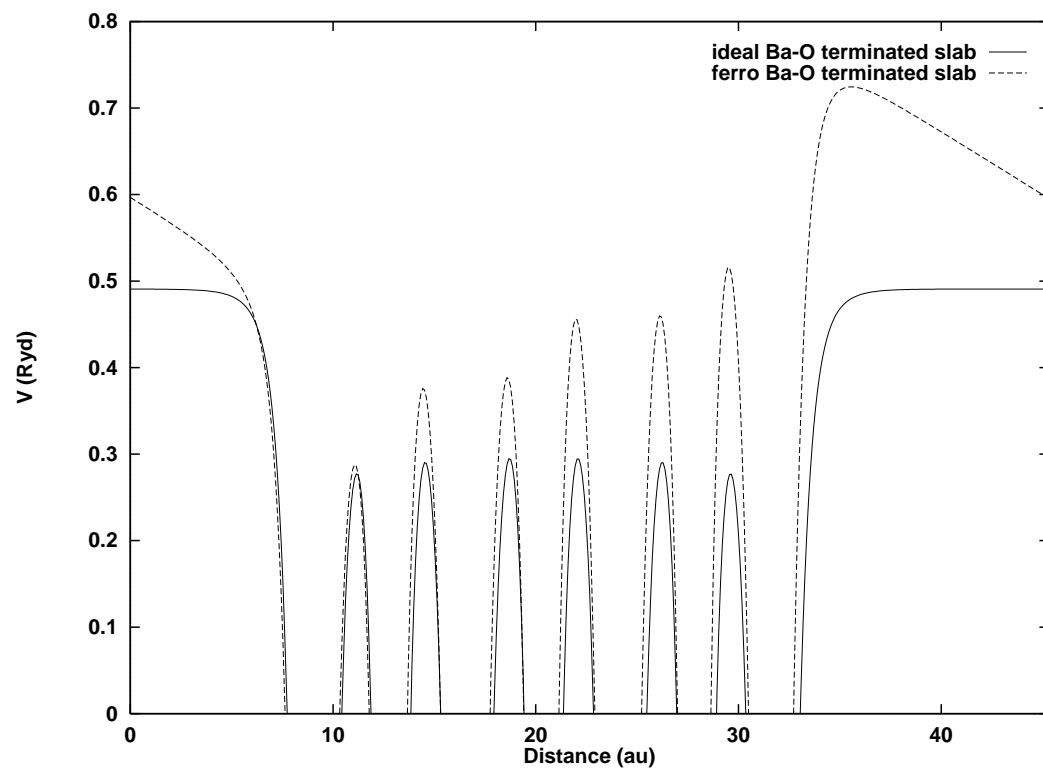


Fig. 9 Cohen

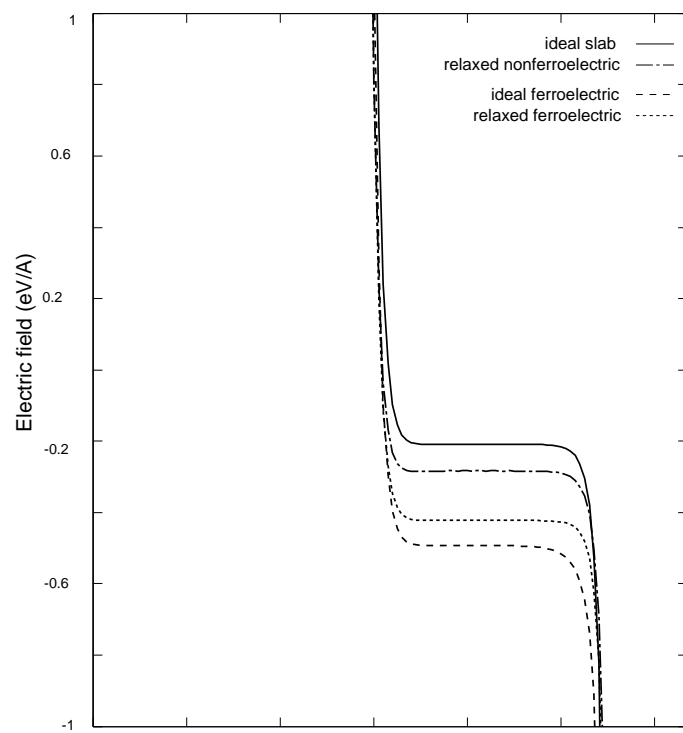


Fig. 10 Cohen

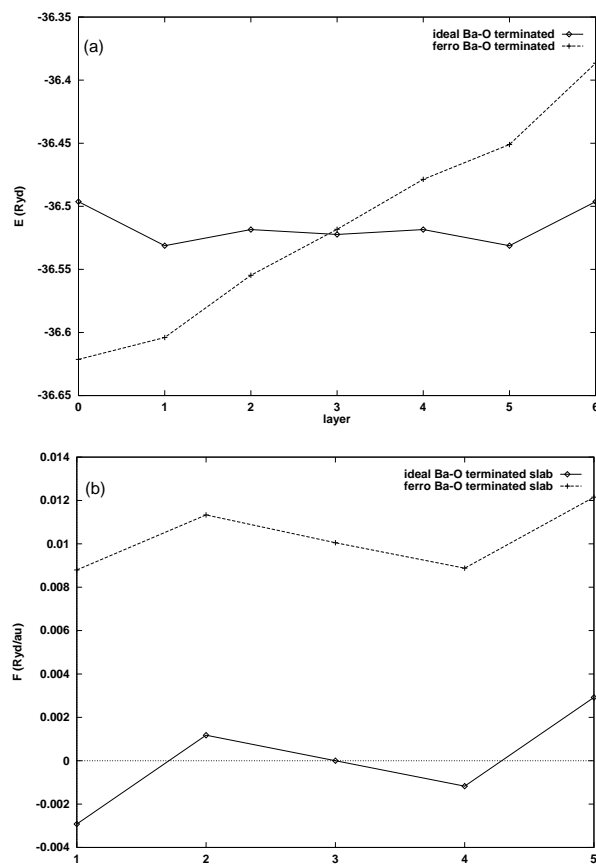


Fig. 11 Cohen

